University of Benghazi … Faculty of Education
Journal of Faculty Education … The nineteen number…December 2025

Study on the Effect of Nb Doping on the Structural and Optical Properties of Barium Titanate Perovskite Nanocrystals

[*a] Dr. Mohammed Awadh Saeed Al-Ameri
[b] Aisha Ali Mohammed Al-Sharif

[a, b] Department of Physics -Faculty of Education -Seiyun University- Seiyun-Hadhramout-Yemen

(Material Science Physics)

دراسة في تأثير التطعيم بالنيوبيوم على الخصائص البصرية والتركيبية في البلورات النانوية من بيرفسكايت تيتانات الباريوم

*[1] د. محمد عوض سعيد العامري

أستاذ مساعد

[2]عائشة علي محمد الشريف

1,2 قسم الفيزياء– كلية التربية – جامعة سيئون – سيئون–حضرموت– اليمن

(فيزياء علم المواد)

malameri301984@gmail.com

ABSTRACT

In this paper, five samples of perovskite oxide nanocrystals with the formula ($Ba\ Ti_{(1-x)}\ Nb_{(x)}O_3$), where (x = 0.1, 0.2, 0.3, 0.4, and 0.5%), were synthesized using the solid-state reaction method and calcined at 1200°C. All samples were investigated using XRD and UV-Vis spectroscopy. The XRD patterns of the prepared samples with varying Nb compositions showed that the nanopowders have a tetragonal phase. The lattice constants were found to be 0.041, 0.081, 0.122, 0.162, and 0.202 nm, and the particle sizes were determined to be 2.93, 5.80, 8.79, 11.72, and 14.65 nm, respectively. The structural analysis suggests that Nb doping and calcination influence atomic positions and site occupation in the crystal lattice due to differences in the size and charge that results in direct changes in the optical, structural and electrical properties of samples during the calcination process in barium titanate. UV-Vis spectroscopy confirmed the optical characteristics of the compounds within the 400–800 nm range. The energy gap of the nanocrystal samples was calculated, showing that the highest value of Eg was 3.30 eV, while the lowest value was 3.16 eV. The following optical properties, like absorption, optical absorption coefficient, extinction coefficient, refractive index, reflectance, transmittance, and optical conductivity were calculated as functions of wavelength. The variations in the optical properties might be attributed to the varying Nb content in the prepared samples. In addition, changes in grain size and phase transitions play a significant role in modifying the energy levels, which in turn greatly affect the optical measurements of these samples.

Keywords: Energy gap, patterns, XRD, UV-visible, spectroscopy.

الملخص

في هذه الورقة العلمية، خمس عينات من أكاسيد البيروفسكايت النانوية التركيب ذات الصيغة الكيميائية ($Ba\ Ti_{(1-x)}\ Nb_{(x)}\ O_3$) وذلك عندما تكون (**x** = 0.1، 0.2، 0.3، 0.4، و0.5%) التي تم تحضيرها بطريقة تفاعل الحالة الصلبة وتم تكليسها عند درجة حرارة (1200 درجة مئوية). جميع العينات تم التحقق منها من خلال تقنيات طيفية مثل مطياف حيود الأشعة السينية ومطياف الأشعة المرئية فوق البنفسجية. نتائج أنماط مطياف حيود الأشعة السينية لعينات مركب تيتانات الباريوم المشوبة بكميات مختلفة من عنصر النيوبيوم أثبتت أن المساحيق النانوية لها طور رباعي، وكذلك ثوابت الشبيكة وجدت عند القيم (0.041، 0.081، 0.122، 0.162،و 0.202) بوحدات النانو على التسلسل، وكذلك حجم الحبيبات تم اكتشافه عند القيم (2.93، 5.80، 8.79، 11.72، و14.65) بوحدات النانومتر على التوالي. قد تكون النتائج المستخلصة من الخصائص التركيبية مرتبطة إرتباطا وثيقا بالتغيرات في مواقع الذرات بعنصر النيوبيوم (Nb) في تيتانات الباريوم ($BaTiO_3$) في الشبكة البلورية بسبب اختلاف الشحنة والحجم، مما يؤثر مباشرة على الخصائص البصرية، البنيوية، والكهربائية للعينة، وكذلك بإحتلال الذرات لمواضعها خلال عملية التكليس. الخصائص البصرية للمركبات الجديدة تم الوصول إليها باستخدام تقنية مطياف الأشعة المرئية فوق البنفسجية عند الأطوال الموجية ضمن المدى (400–800 نانومتر). كما أن فجوة النطاق للعينات النانوية تم حسابها، حيث كانت أعلى قيمة لها (3.30 الكترون فولت)

بينما كانت أقل قيمة عند (3.16 الكترون فولت). الخصائص البصرية الآتية: الامتصاصية ، معامل الامتصاص البصري، معامل التوهين، معامل الانكسار ، الانعكاسية ، النفاذية ، والموصلية البصرية تم حسابها كدوال بالنسبة للطول الموجي. قد يعزى التغير في الخصائص البصرية إلى إختلاف محتوى عنصر النيوبيوم (Nb) في العينات المحضرة. بالإضافة إلى ذلك، فإن التغيرات في حجم الحبيبات والتحولات بين الأطوار البلورية تلعب دورا كبيرا في تعديل مستويات الطاقة، مما يؤثر بشكل كبير على القياسات البصرية لهذه العينات.

كلمات مفتاحية: فجوة النطاق، أنماط، حيود الأشعة السينية، الأشعة المرئية فوق البنفسجية، الطيف.

Introduction:

Since the early 1940s, following the discovery of barium titanate as the first oxide compound with a perovskite structure exhibiting ferroelectric behavior, it has been utilized in a wide range of scientific and industrial applications (Aktaş, 2020), and (S. Alex Pandian, M. Sivakumar, 2023). Due to its versatility, barium titanate has become one of the most significant electroceramic materials among ferroelectrics (Fatima Basil, et al.,2022). Its ferroelectric properties are connected with three structural phase transitions: from orthorhombic to tetragonal (-90°C to 5°C), tetragonal ferroelectric (5°C to 120°C) to cubic Para electric (T>120°C) structure (Fakhar-e-Alam, et al., 2023) , (Mahata et al., 2020), and (Ahamed et al., 2020).

Barium titanate ($BaTiO_3$) nanoparticles, a ceramic material of the perovskite type, possess remarkable properties, including a high dielectric constant along with ferro-, piezo-, and pyroelectric characteristics (Ping, et al., 2021). The $BaTiO_3$ nanoparticles are widely utilized in the production of multilayer ceramic capacitors, thermistors, transducers, infrared detectors, sensors, and electro-optical devices (Karvounis et al., 2020).

Nanotechnology captivates many researchers due to its unique physical, chemical, and structural properties, and it can be applied in various scientific fields, including physics, chemistry, material science, and medicine (Sumanasinghe, 2023), and (Baudry, 2022). Materials at the micrometer scale do not exhibit significant changes in physical properties when compared to their bulk counterparts (Razzak, et al., 2022), and (Nguyen, 2020). However, materials at the nanoscale show drastic changes in their physical properties (M, et al., 2023), and (Sood, et al., 2023). A material that undergoes minimal changes in its physical properties in bulk form will exhibit varying physical and chemical properties when reduced to the nanoscale (Ahamed, et al., 2020). These properties include thermal behavior, stability, solubility, and conductivity (Jebli et al., 2021).

Nanomaterials have diverse applications in both the electronics and biomedical industries (Angelats-Silva, et al., 2022). Their unique properties make them highly valuable in biomedical applications such as drug delivery, biosensors, and cell detection (Nandi, 2020). Nanomaterials are categorized based on their dimensions: nanoparticles (zero-dimensional), nanorods and nanowires (one-dimensional), and thin films and nanosheets (two-dimensional) (Batoo et al., 2021).

Structurally, the nanoprobes used for diagnosis and imaging are core-layer nanocomposites, with a ferroelectric core encased in a biocompatible layer (Zhou, 2022). It is

important to note that barium titanate nanoparticles must exceed a certain critical size to maintain their ferroelectric properties (Gigli et al., 2022), and (Yoon et al., 2020).

According to research by Bhat et al., 2020, barium titanate was doped with (Rh). The findings suggested that doping barium titanate with Rh lowered the photon energy, which impaired electronic properties while enhancing its photocatalytic activity (Bhat et al., 2020). Furthermore, ytterbium was added to $BaTiO_3$ to enhance the electrical and optical properties and increase dielectric constats (Alshoaibi et al., 2020). $BaLaTiO_3$ powders were formed using the sol-gel route. X-ray and IR spectroscopy proved the chemical bonds while increasing La content caused transition of the tetragonal into the cubic phase and increased grain sizes during the chemical process. The La value will increase until it reaches a maximum value at 21000 (Aleksandova et al., 2021). The solid-state reaction method was used to study the effect of Calcium doping in $BaTiO_3$, and the results proved that the formation of the tetragonal phase and perovskite structure. The microscopy observation showed non-uniformity in the powders and significant variations in the grain sizes. Additionally, the new samples exhibited two transitions between 150 $^{\circ}$C to 500 $^{\circ}$C in the temperature range (T.O. Daniel et al., 2025).

The purpose of this paper is to synthesize a new material with chemical formula of ($BaTi_{(1-x)}\ Nb_{(x)}O_3$), where the molar fraction (x = 0.1, 0.2, 0.3, 0. 4, and 0.5%), using solid-state reaction method. The structural and optical results were proved using XRD and UV-Visible spectroscopy techniques.

The goal of this research is to create new knowledge in the areas of materials science and physics that can also be useful for a variety of manufacturing and industrial applications. Prior work has shown that doping $BaTiO_3$ with Rh, Yb, La, or Ca can dramatically change structural, optical, and electrical properties, including grain size, phase transitions, and band gap. To build on the previous work, the current study examines Nb doping of $BaTi_{(1-x)}\ Nb_{(x)}O_3$ (x = 0.1–0.5%) using solid-state reaction methods and also considers structural and optical properties. Nb doping is anticipated to create new lattice distortions and optical transitions that have not been reported before. These areas are key to the originality and importance of the current work.

Experimental details:

Barium carbonate ($BaCO_3$), titanium dioxide (TiO_2), and niobium dioxide (NbO_2) with 99.99% purity were used to prepare ($BaTi_{(1-x)}\ Nb_{(x)}O_3$) nanocrystals using the solid-state reaction method with Nb doping levels varying from 0.1 to 0.5. In all cases, 2 grams of powders were blended with acetone in a mortar for 2 hours to obtain a homogenous mixture, preheated at 200°C for 4 hours, remixed with acetone for 1 more hour, and the powders were calcined at 1200°C for 5 hours to complete the reaction, utilizing the same mixing procedure for all five compositions (UL Hag et al., 2022). The X-ray diffraction (XRD) patterns were acquired in the 20°–80° 2θ range at 40 kV to study the structural parameters, and the UV-Visible absorption spectra were obtained for the solutions by dissolving 0.01 g of each sample powder in 10 mL of distilled water, scanning from 200 to 800 nm, using distilled water as a blank (Al-Ameri et al., 2022). These studies produced the structural and optical parameters of the powders including crystallinity, lattice constants, grain size, absorption coefficient, refractive index, transmittance, and reflectance can be calculated from the following equations:

$$\frac{1}{d^2} = \frac{4}{3}\left(\frac{h^2+hk+k^2}{a_\circ^2}\right) + \left(\frac{l^2}{c_\circ^2}\right) \quad \text{..... (1)}$$

$$D_{av} = \frac{0.9\lambda}{B\cos\theta} \quad \ldots\ldots (2)$$

$$\alpha = 2.303A/t \quad \ldots\ldots (3)$$

$$K = \lambda\alpha/4\pi \quad \ldots\ldots (4)$$

$$(\alpha h\nu)^2 = C(h\nu - Eg) \quad \ldots\ldots (5)$$

$$n = \frac{(1+\sqrt{R})}{1-\sqrt{R})} \quad \ldots\ldots (6)$$

$$R = \frac{1}{\log 10^{A}} \quad \ldots\ldots (7)$$

$$T = 1 - R - A \quad \ldots\ldots (8)$$

$$\delta_{op} = \frac{\alpha nc}{4\pi} \quad \ldots\ldots (9)$$

In this investigation, the symbols and parameters defined below will be employed: (h,k,l) means the Miller indices, B denotes the full width at half maximum (FWHM), λ is wavelength, $a_{\circ}, c_{\circ}, d$ are lattice constants, A is the absorption, and (t) is the thickness of the sample, K is the extinction coefficient, (4π) is a constant, C is constant, n is the refractive index, R is the reflectance, T is the transmittance, δ_{op} is the optical conductivity, α is optical absorption coefficient, and c is the speed of light in the vacuum. These definitions are found from previous studies (Al-Ameri et al., 2020; Phong et al., 2022; Saxena et al., 2021; Zhang et al., 2023; Al-Ameri, 2023, 2024).

Results and Discussion:

The XRD Results:

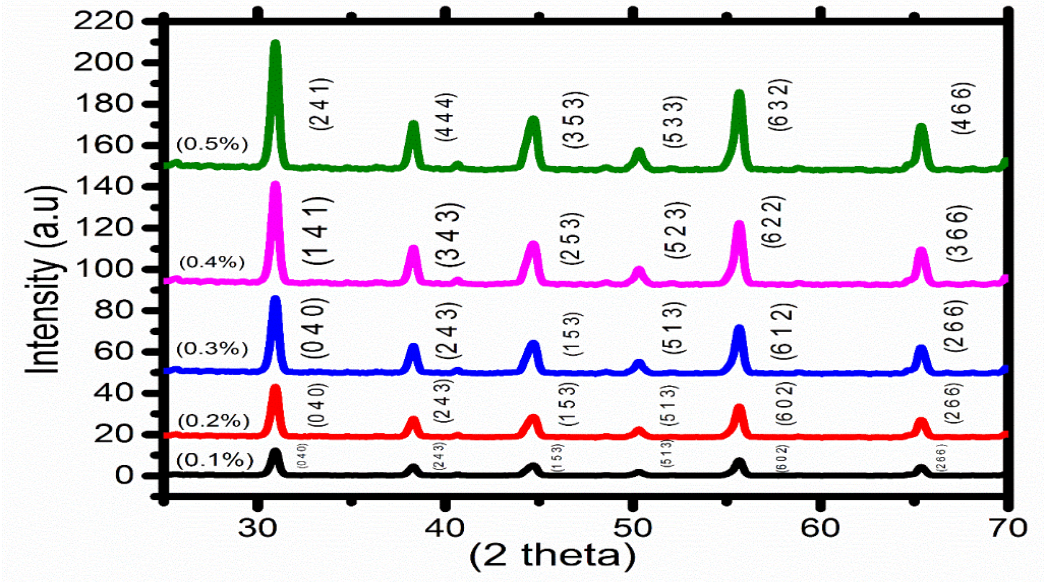

Fig. (1). The XRD patterns for nanocrystal

Table (1). The XRD results of the nanocrystals:

No	Lattice Constants (nm)	Particle Sizes (nm)	Peak Positions (nm)	Chemical Phase	α,β,γ
1	0.041	2.93	47.15	tetragonal	90
2	0.081	5.80	46.47	tetragonal	90
3	0.122	8.79	47.30	tetragonal	90
4	0.162	11. 72	44.88	tetragonal	90
5	0.202	14.65	47.50	tetragonal	90

Figure (1) and table (1) display the diffraction peaks of ($Ba_{(1-x)}$ $Nb_{(x)}O_3$) nanopowders. The XRD results proved that the chemical phase is tetragonal and the perovskite form invaginated at the calibrated peak that can be found at 30°. The five synthesized powders all displayed a pronounced peak at 30.76°, 30.88°, 30.88°, 30.88°, and 30.88° respectively. Each sample displayed a distinct broad peak at a 2θ range of around 44.62° - 44.66°. The results may be related to the radii and the dopant amount in the barium titanate (Nahar et., 2021). Increasing Nb to higher peak intensities, which is attributed to in ionic radius and ion density (Elius et al., 2020). Grain sizes and the lattice constants were measured to range from 0.041 to 0.202 nm and 29.3 to 14.65 nm, respectively. Peak positions for all samples were calculated between 44.88° and 47.50°. These variations could be to changes after Nb doping. No significant shifts in diffraction peaks were observed. Likely because Nb content is very low (More et al., 2020). Rietveld refinement was applied to all samples to determine lattice constants, atomic position, and occupation. The analysis of confirmed the tetragonal perovskite structure as the most stable phase, with Nb partially substituting Ti atoms (Batto et al., 2021). The refinement of the peak profile using the microstructural models allowed accurate estimation of grain sizes, explaining the peak broadening near 44.6° (Tomar et al., 2020). Also, phase fraction analysis showed that only the preovskite phase was present, with no detectable secondary phase. Rietveld refinement validated the observed results, including, peaks positions, peak widths, grain sizes, lattice contestant, and chemical phases (Aktas, 2022).

3.2. The UV-Visible Results:

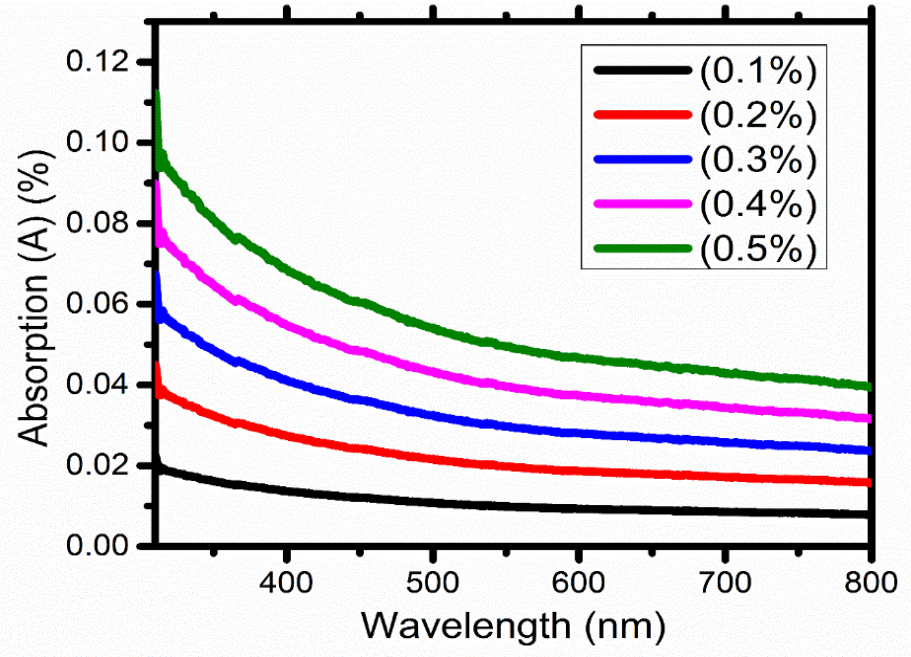

Fig. (2). The variations of wavelength for nanocrystal

Figure (2) illustrates the absorption of prepared samples as a function of wavelength. The maximum absorption values were measured to be 0.02%, 0.04%, 0.06%, 0.078%, and 0.094% at wavelength near 311 nm. The sudden decrease in values of the absorption can happen at wavelengths below 500nm, and the stable values of absorption were noted above 500 nm. These results may be related to the major absorption edge, the increase in grain size, and the decrease in the number of defects in the synthesized samples (Iriani, et al., 2022). The absorption peak found at 311 nm is associated with the major optical transition within at the band edge, which also introduces the energy gap of the material. The increase of absorption with Nb content signifies doping defines additional electronic states. The decline in the absorption values below 500 nm depicts the occurrence of higher energy electronic transitions and the depletion of states for photons to interact; the stability of absorption results at 500 nm and above implies minimal interband transitions. Each of these observed behaviors demonstrates structural enhancements including larger grain size and fewer defect density directly contribute to the optical performance of the nanopowders (Menasre, et al., 2024).

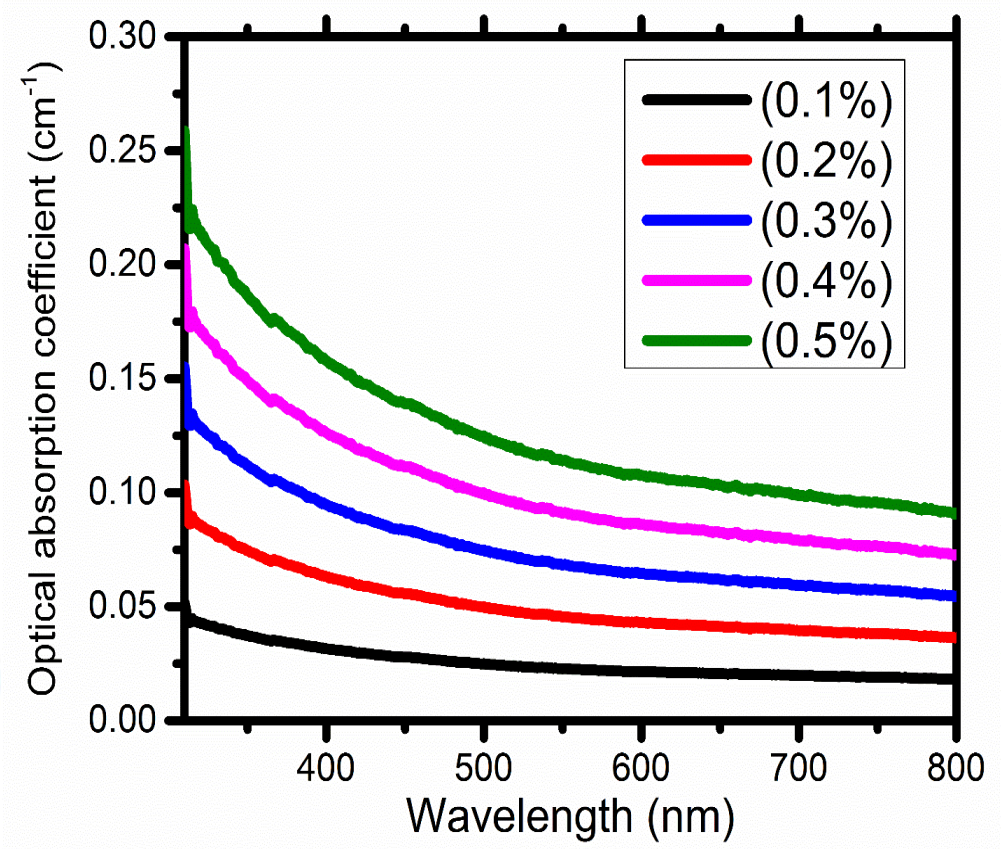

Fig. (3). The variations of (α) with (λ) for nanocrystal

Figure (3) explains the optical absorption coefficient of the synthesized samples as a function of wavelength. The maximum optical absorption coefficient values were calculated to be 0.046, 0.09, 0.13, 0.18, and 0.22 cm^{-1}consecutively at wavelength near 311 nm. After that, the (α) values were decrease suddenly below 500 nm, and these results were more stable at wavelengths above 500 nm. These results may be related to the increase in grain size and the decrease in the number of defects in all prepared samples, and the increase in the doping ratio led to a clear increase in all values of the optical absorption coefficient at low energies (Karvounis A. et al., 2020). The primary absorption edge transitions to lower photon energies, suggesting that the effective band gap is reduced, which may be relate to the presence of enhanced density of state and shallower defect levels (Tihtih M. et al., 2022). The hard reduction of α below 500 nm proposes that new higher energy transitions occur with slight accessible electronic states; conversely, the constancy of α signifies low intermixed band switching above 500 nm., these optical characteristics suggest a strong relationship between structural impurities and grain size, improved crystallinity, decrease in defects, and improved inter-viad electronic transitions, caused by Nb doping on the optical characteristics of the nanocrystals, and the major absorption edge shifts towards lower photon energies (Palusamy et al., 2023).

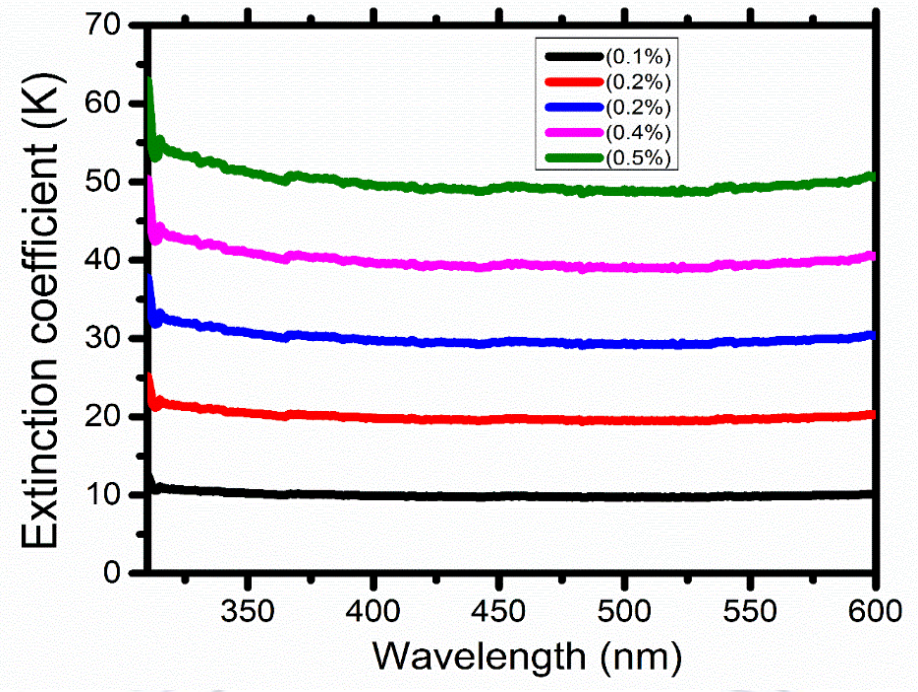

Fig. (4). The variations of (K) with (λ) for nanocrystal

Fig. 4 shows the extinction coefficient of the prepared samples as a function of wavelength. The maximum optical absorption extinction coefficient values were given to be 11.33, 22.4, 34.18, 44.3, and 54.7, respectively at 311 nm. The (K) values showed a slow decrease in the (λ) range below 350 nm, this means that the transition must correspond to a direct transition, and the properties of this state are very important, as they are responsible for electrical conduction (Bo¨ ttcher et al., 2021). These results may be related to the increase in grain size and the decrease in the number of defects, which led to a clear increase in all values of (A) and (α), which in turn affected the (K) values (Hassan et al.,2023). The steadily rising way in K with higher doping levels denotes that Nb incorporation cements a greater quantity of available electronic states capable of contributing to direct transitions, resulting in an increased ability for these materials to interact with incident photons. The ultimate decline that occurs below 350 nm is due to higher-energy transitions occurring with scarce available density of state. The constant K value above 350 nm, confirms that electronic states at lower energy are more stable. These types of behavior confirm the relationships between structural advancements in larger grain size and reduced defects, with the improvement in optical response, confirming that direct transitions dominate conduction-related optical transitions in these Nb-doped nanocrystals (Tihtih et al., 2020).

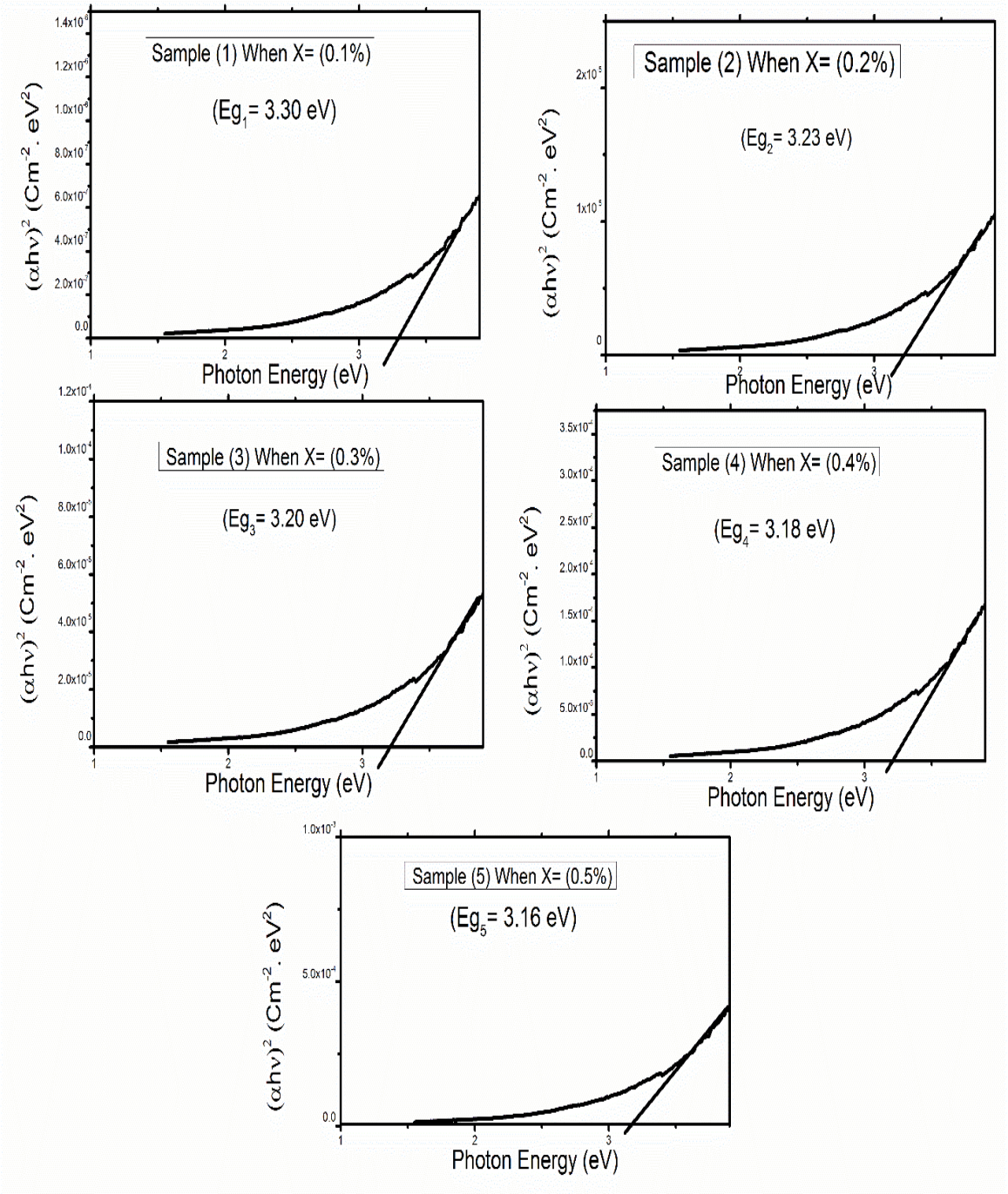

Fig. (5). The (Eg) values for nanocrystal

By plotting $(\alpha h\nu)^2$ and the photon energy as shown in Fig. 5, and extrapolating the straight thin portion of the curve to intercept the energy axis, the photon energy was calculated. The values of (Eg) were found to be 3.30, 3.23, 3.20, 3.18, and 3.16 eV, respectively. The decrease in (Eg) may be related to the reduction in grain boundaries and their density due to the heating effect on the nanocrystal samples (Abed et al., 2024). The gradual depression in Eg with rising Nb doping indicates that the Nb ions suggests the number of electronic states or defect levels close to the conduction band, which, in turn, leads to band narrowing. As well, a higher degree of crystallinity and larger grain sizes will lower the number of grain boundaries, thus lower carrier scattering and resulting in more delocalized electronic states, and allowing absorption of photons with lower energy. This

behavior illustrates the important relationship between the structure and electronic properties, reaffirming that both doping and thermal treatment have an important role in modifying the optical band gap of the nanocrystals (Tihtih M. et al., 2023).

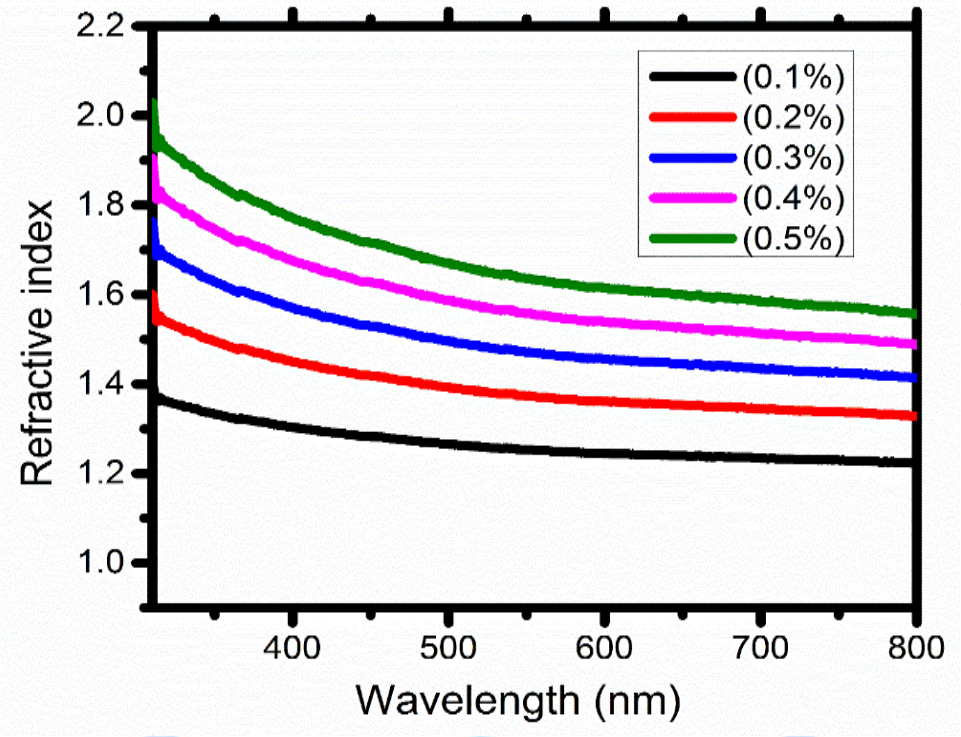

Fig. (6). The variation of (n) with (λ) for nanocrystal

Fig. (6) displays the refractive index of the nanocrystals samples a function of wavelength. The maximum results of the refractive index were noted to be 1.4, 1.55, 1.7, 1.8, and 1.94, respectively at 311 nm. Following this, the (n) values exhibited a sharp decline in the (λ) range below 500 nm with various values of (n). The refractive index values remained stable for (λ) greater than 500 nm. This means that the increase in the dopant quantity in ($BaTiO_3$) may be related to the fact that synthesized samples became less transparent with the increasing Nb content. The increase in the refractive index with higher Nb loading suggests that doping modifies the electronic polarizability of the material by introducing additional localized electronic states. The sharp decrease of refractive index below 500 nm may be related to high energy transitions where light photon energies exceed the effective band gap, which results in a little refractive response. The consistency of refractive index above 500 nm suggests that low energy photons while the gradual convergence to the refractive index of undoped $BaTiO_3$ indicates the influence that Nb induced structural and electronic changes have on optical density. These trends indicate a strong correlation between increased doping, decreased transparency, and increase electronic polarizability, validating Nb's role in modifying the optical properties of the nanoceramic powders (Marz ouk et al., 2022).

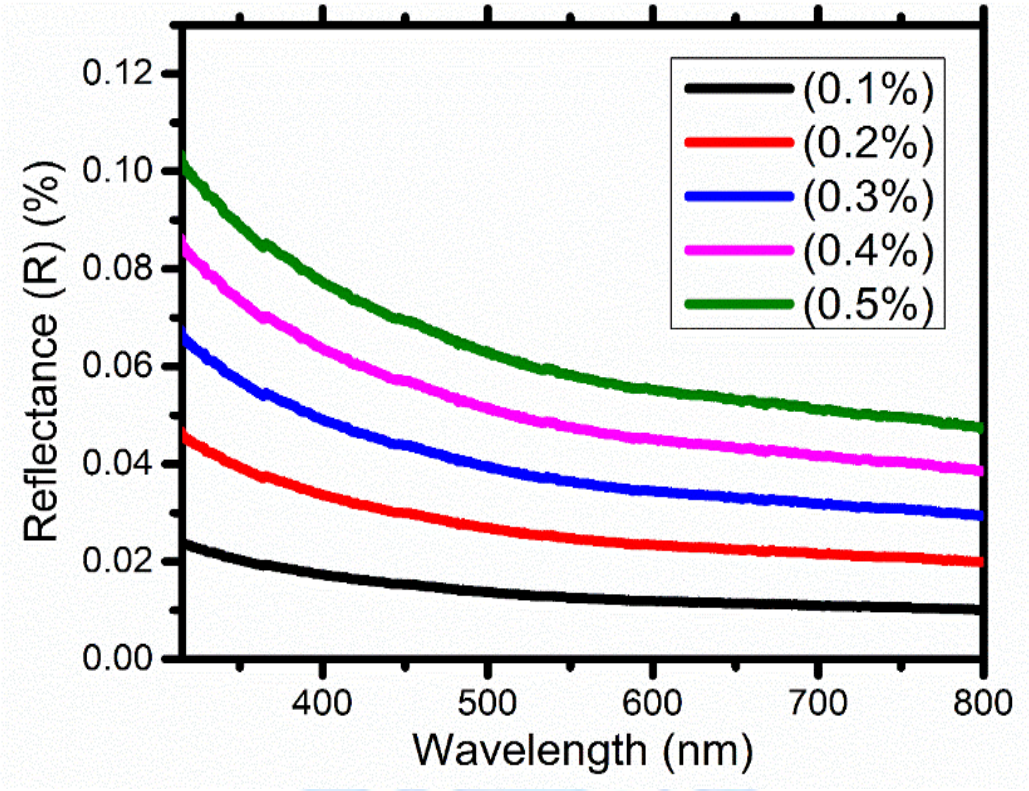

Fig. (7). The variations of (R) with (λ) for nanocrystal

Fig. (7) displays the reflectance of the prepared samples as a function of wavelength. The maximum results of the reflectance were measured to be 0.023, 0.045, 0.066, 0.083, and 0.1%, respectively at 311 nm. The (R) values were increased quickly at the range below 500 nm, and the (R) remained constant at (λ) greater than 500 nm. The gradual increment of reflectivity with higher Nb content implies that doping evolves the surface electronic states, which increases light absorption and lowers the number of photons being reflected. The steep drop of R-below 500nm indicates higher-energy electronic transitions where higher-energy photons are absorbed more efficiently by the material. The plateau R, invariant with photon energy above 500nm, indicates all lower-energy photons are absorbed, and the sample's reflectivity has plateaued. This information supports the strong interaction between structural modifications induced by Nb, namely enhanced grain size and lower defect concentration, and the optical properties of the samples. Certainly, Nb doping not only modifies sample absorption and refractive index, but systematically modulates the sample surface reflectivity via tunable electronic structure of the nanocrystals (Rini et al., 2024).

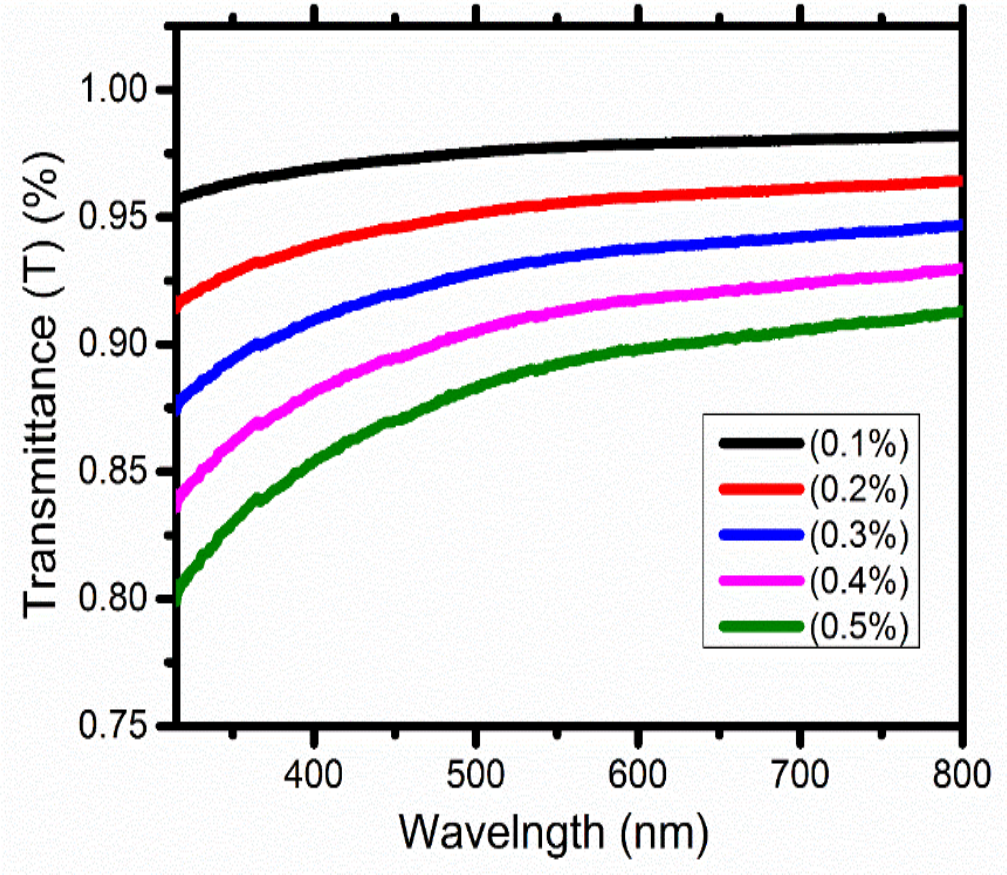

Fig. (8). The variations of (T) with (λ) for nanocrystal

Fig. (8) shows the transmittance of the prepared samples a function of wavelength. The maximum results of the refractive index were calculated to be 0.96%, 0.92%, 0.78%, 0.84%, and 0.80%, respectively, at a constant wavelength of at 315 nm. These values of (T) were followed by a sudden increase for (λ) less than 600 nm, and the (T) values remained stable for (λ) greater than 600 nm. The high transmittance values indicate that the dopant in all prepared nanoceramic samples of barium titanate may be responsible for the increased transmittance with the addition of Nb content. The proved in transmittance with increasing Nb content implies that doping minimizes scattering points and defects in the nanocrystals, allowing for greater propagation of photons through the material. The abrupt increase of T below 600 nm is consistent with improved absorption of high-energy photons and less trapping of photons at grain boundaries. The stability of T above 600 nm reflects the influence of an intrinsic lattice transparency associated with lower-energy photons. Overall, these behaviors illustrate the contributed forces of better crystallinity, larger grain size, and controlled defect density on optical transmittance. In summary, Nb doping is a viable method of systematically manipulating the transmittance and photon transport characteristics of the nanoceramic powders (Islam et al., 2022).

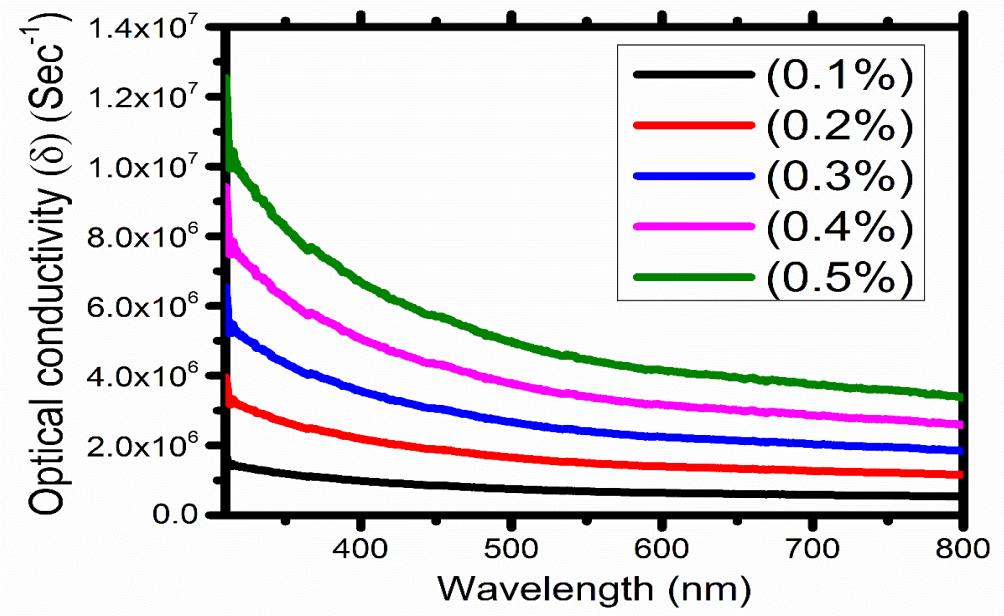

Fig. (9). The variations of (δ) with (λ) for nanocrystal

Fig. (9) explains the optical conductivity of the nanocrystals samples a function of wavelength. The maximum values of the optical conductivity were found to be (1.4×10^6, 3.5×10^6, 5.6×10^6, 7.7×10^6, and 10.1×10^6 Sec^{-1}), respectively at 311 nm. These values were followed by a sudden decrease for (λ) below 500 nm, with varying values of. Subsequently, and the remained stable for (λ) above 550 nm. These results may be related to the increase in grain size and the decrease in the number of defects. Additionally, the results showed that the decrease in values of (T) led to a clear increase in the (δ_{op}) (Ali et al., 2020). The trends displayed in δ indicate that increased Nb doping promotes energy dissipation mechanisms in the nanocrystals, which is likely a result of the heavier polarization and interaction of incident photons with localized defect states. The abrupt drop of δ below 500 nm represents less opportunity for high energy electronic transitions to occur, while the consistent δ value above 550 nm shows equilibrium with the dielectric loss at lower photon energies. The correlation between T and δ, indicates that decreased photon transmission due to absorption or scattering leads to energy dissipation via dielectric loss. In addition, these behaviors highlight the strong coupling between structural optimization larger grain sizes, less defects, etc. and the dielectric response, which emphasizes the important role of Nb doping in adjusting both optical and energy dissipation properties of the nanoceramic powders (Hassan, et al., 2023).

The optical properties of Nb doped $BaTiO_3$ samples are dependents on their structural properties. Increased Nb content led to larger grain sizes and lower defects, which increased electronic transitions, photon absorption, and the electronic density of states related to direct and indirect transitions. The changes manifest in absorption, absorption coefficient, extinction coefficient, refractive index, reflectance, transmittance, and dielectric loss experienced a shift in the absorption edge while lowering the effective band gap, with improved scattering of photons and improved energy transport. This suggests the controllability of crystal structure with Nb doped $BaTiO_3$ samples serves as an important advantage for improving optical-electronic properties. This research into Nb doped $BaTiO_3$ nanocrystals illustrates the novelty of the research by introducing its innovative preparation method that produced distinct microstructures, uniform grains, and diminished defects that improved optical and electrical properties. The findings also indicate that the Nb doping concentrations used resulted in significant enhancements to the absorption, band gap, refractive index, and dielectric loss

compared to other doped materials. Additionally, new mechanistic findings into Nb's impact on structural and optical properties were demonstrated, emphasizing the relevance of crystal structure and appropriate doping to achieve improved functional performance with the nanocrystal samples.

4. Conclusion:

All the synthesized compounds were obtained by solid-state synthesis and all the samples were doped with Nb atoms. Subsequently, all of the films were characterized by XRD and UV–Vis techniques. The XRD test results revealed that the tetragonal phases were identified and it shows that average lattice constants approach into different amount of Nb atoms in these prepared samples, 0.041 nm-0.202 nm, grain sizes ranges from 2.93nm - 14.65nm for all samples. The UV-visible determination of photon energy has resulted in higher at 3.30 eV and lower was found to be near by 3.16. Another optical property، such as absorption, optical absorption coefficient, extinction coefficient, refractive index, reflectance and transmittance and optical conductivity were calculated as a function of wavelength.

6.References:

Islam, S., Khatun, N., Habib, M. S., Farhad, S. F., Tanvir , N. I., Shaikh, M. A., Siddika , A. (2022). Effects of yttrium doping on structural, electrical and optical properties of barium titanate ceramics. Heliyon, 01(01), 1-9. doi:https://doi.org/10.1016/j.heliyon.2022.e10529.

Rini, R. P., Nurosyid, F., Iriani, Y., & Fasquelle, D. (2024). The addition of bismuth (Bi) to the barium titanate (BaTiO3) prepared by chemical solution deposition. Journal of Physics: Conference, 1825(012065), 1-10. doi: 10.1088/1742-6596/1825/1/012065.

Sood, A., Desseigne, M., Dev, A., Maurizi, L., Kumar, A., Millot, N., & Han, S. S. (2023). A Comprehensive Review on Barium Titanate Nanoparticles as a Persuasive Piezoelectric Material for Biomedical Applications: Prospects and Challenges. Hal Open Sceince, 19(12), 2206401. doi: f0.1002/ smll.202206401.

Tihtih, M., Ibrahim, J. F., Basyooni, M. A., En-nadir, R., Belaid, W., Abdelfattah, M. M., Kocserha, I. (2023). Enhanced optical and thermal conductivity properties of barium titanate ceramic via strontium doping for thermo-optical applications. Optical and Quantum Electronics, 55(226), 1-20. doi:https://doi.org/ 10.1007/ s11082-022-04516-8.

Abed , N. Z., Ismail, R. A., & Shaker, S. S. (2024). Role of substrate temperature on the performance ofBaTiO3/Si photodetector prepared by pulsed laser deposition. Scientifc Reports, 14(453), 1-16. doi: https:// doi.org/ 10.1038/ s41598-024-55053-1.

Ahamed, M., Akhtar, M. J., Khan, M. M., Alhadlaq, H. A., & Alshamsan, A. (2020). Barium titanate (BaTiO3) nanoparticles exert cytotoxicity through oxidative stress in human lung carcinoma (A549) cells. Riyadh-11451,: King Abdullah Institute for Nanotechnology. https://dx.doi.org/10.4314/dujopas.v9i3a.13.

Aktas, S. Z. (2020). Structural investigation of barium zirconium titanate Ba(Zr0.5Ti0.5)O3 particles synthesized by high energy ball milling process. J. Chem. Sci., 132(130), 1-8. doi:https:// doi.org/ 10.1007/ s12039-020-01837-7.

Al-Ameri, M. A. (2022). The Effect of Sunlight Exposure on Physicochemical Properties of Plastic Bottled Water at Al-Mogran Station in Khartoum State, Sudan. ARID

International Journal for Science and Technology (AIJST), 5(10), 130-143. doi:https:// doi.org/10.36772/arid.aijst.2022.5106.

Al-Ameri, M. A. (2023). The Effect of Heat and Storage Duration on Physicochemical Properties of Plastic Bottled Water at Sharq El Nile Locality in Khartoum State, Sudan. ARID International Journal for Science and Technology (AIJST), 6(12), 54-69. doi:https:// doi.org/ 10.36772/ arid.aijst.2023.6123.

Al-Ameri, M. A. (2024). Preparation and Characterization of (Ba(0.99) Fe(0.01) Ti(0.99) Zr(0.01)O3) Nanostructure Perovskite using Energy Dispersive X-ray Microanalysis and Laser Induced Breakdown Spectroscopy Techniques. SHU Journal for Humanities and Applied Sciences, 2(1), 220-229. Retrieved from https:// shu.edu.ye. http://dx.doi.org/10.18576/ijtfst/110307.

Al-Ameri, M. A., Ahmed, S. A., & Babikier, M. H. (2020). ynthesis and Optical properties of (Ba(1-x) Mgx Ti(1-x) Mnx O3) Single Preovskite Oxide. European Journal of Advances in Engineering and Technology, 7(2), 20-22. Retrieved from Available online www.ejaet.com. https://doi.org/10.1016/j.matpr.2020.07.646.

Ali, A., Uddin, S., Zaman, A., Ahmad, A., Kamran, M., & Iqbal, Z. (2020). Dielectric and Optical Properties of Tin-doped Barium Tetra Titanate Ceramics. Revista Română de Materiale / Romanian Journal of Materials, 50(04), 448 - 452. https:// doi.org/ 10.48048 /wjst .2021. 9944.

Angelats-Silva, L. M., Pérez-Azahuanche, F., Roldan-Lopez, J. A., Emelianov, N. A., Céspedes-Vásquez, R. B., & Valverde-Alva, M. A. (2022). Infuence of the surface modifcation of BaTiO3 nanoparticles by hydrolyzed chitosan obtained from shrimp exoskeletons on the optical response intensity of the second harmonic. MRS Advances, 7(1), 260–264. doi:https:// doi.org/ 10.1557/s43580-022-00278-3.

Angelats-Silva, L. M., Pérez-Azahuanche1 , F., Roldan-Lopez1, J. A., Emelianov, N. A., Céspedes-Vásquez, R. B., & Valverde-Alva, M. A. (2022). Infuence of the surface modifcation of BaTiO3 nanoparticles by hydrolyzed chitosan obtained from shrimp exoskeletons on the optical response intensity of the second harmonic. MRS Advances, 7(1), 260–264. doi:https:// doi.org/ 10.1557/s43580-022-00278-3.

Batoo, K. M., Verma , R., Chauhan, A., Kumar, R., Hadi, M., Aldossary, O. M., & Al-Douri d, Y. (2021). Improved room temperature dielectric properties of Gd3+ and Nb5+ co-doped Barium Titanate ceramics. Journal of Alloys and Compounds, 838(160838), 1-21. doi:https:// doi.org/ 10.1016/ j. jallcom. 2021.160836.

Batoo, K. M., Verma, R., Chauhan, A., Kumar, R., Hadi, M., Aldossary, O. M., & Al-Douri , Y. (2021). Improved room temperature dielectric properties of Gd3+ and Nb5+ co-doped Barium Titanate ceramics. Journal of Alloys and Compounds, 883(160836), 1-21. doi:https:// doi.org/ 10.1016/ j. jallcom. 2021.160836.

Baudry, L. (2022). Coexistence of ferroelectric phases in barium titanate single-domain thin fims. AIP Advances, 12(065205), 1-10. doi:. https:// doi.org/ 10.1063/5.0088519.

Bo¨ ttcher, R., Langhammer, H. T., Walther, T., Ku¨ cker, S., & Ebbinghaus, S. G. (2021). On the incorporation of nickel into hexagonal barium titanate: magnetic properties and electron paramagnetic resonance (EPR). J Mater Sci, 56(01), 4967-4978. doi:doi.org/10.1007/s10853-020-05566-7.

Elius, I. B., Asif, B. M., Maudood, J., Datta, T. K., Zakaria, A. K., Hossain, S., . . . Kamal, I. (2020). Synthesis and Characterization of Strontium Doped Barium Titanates using

Neutron Diffraction Technique. NUCLEAR SCIENCE AND APPLICATIONS, 28(1 &2), 57-62. Retrieved from iftakhar.elius@gmail.com. DOI: 10.1039/ d4ma 005 93g.

Fakhar-e-Alam, M., Saddique, S., Hossain, N., Shahzad, A., Ullah, I., Sohail, A., . . . Saadullah, M. (2023). Synthesis, Characterization, and Application of BaTiO3 Nanoparticles for Anti-Cancer Activity. Journal of Cluster Science, 1(34), 1745–1755. doi:https:// doi.org/ 10.1007/s10876-022-02346-y.

Fatima Basil Sadiq,Hikmat Jameel Abdulbaqi. (2022). The Effect of Nano Barium Titanate on Candida Albicans Adherence and Other Properties of Heat-Cured Soft Acrylic Denture Lining Material. Journal of Research in Medical and Dental Science, 10(10), 109-11. https://doi.org/10.1051/e3sconf/202455301014.

Gigli, L., Veit, M., Kotiuga, M., Pizzi, G., Marzari, N., & Ceriotti, M. ((2022). Thermodynamics and dielectric response of BaTiO3 by data-driven modeling. npj Computational Materials, 8(209), 1-17. doi:https:// doi.org/ 10.1038/s41524-022-00845-0.

Hassan, D., Mohammed, M. K., & Hashim, A. (2023). Exploration the effect of doping (BaTiO3) on optical properties of Polymer (PVP). World Journal of Advanced Research and Reviews, 19(03), 954–963. doi:doi.org/ 10.30574/wjarr.2023.19.3.1845.

Iriani, Y., Suparmi, A., Marzuki , A., & Sandi, D. K. (2022). Microstructures and Optical Properties of Nanocrystalline Pr-doped BaTiO3 Thin Film. International Journal of Thin Films Science and Technology, 11(13), 307-311 . doi:http://dx.doi.org/ 10.18576/ ijtfst/ 110307.

Jebli, M., Hamadoui, N., Rayssi , C., Dhahri, J., Ben Henda, M., & Zaidi, N. (2021). DC-bias dependent impedance and UV-Vis diffuse reflectance spectroscopy of the un-doped and Nb-doped $Ba_{0.9}7La_{0.02}TiO_3$ ceramics. Research Square , 1(1), 1-25. doi:DOI: https:// doi.org/ 10.21203/rs.3.rs-228887/v1.

Daniel, T.O., Okafor, L.C., Arikpo, J.U., Udeh, E., Shaibu, O.D., Edaogbogun, G.O, & Olawale, P.E. Okob. (2025). Synthesis and Characterization of Calcium and Tin Co-Doped Barium Titanate ($Ba_{0.91}Ca_{0.09}Sn_{0.01}Ti_{0.99}O_3$) Application in Ceramic Capacitor. .Chem.Soc.Pak., 47(03), 241-249. DOI: 10.22034/nsam.2024.04.02.

Karvounis, A., Timpu, F., Vogler-Neuling, V. V., Savo, R., & Grange, R. (2020). Barium Titanate Nanostructures and Thin Films for Photonics. Adv. Optical Mater., 08(2001249), 1-23. doi:DOI: 10.1002/adom.202001249.

Karvounis, A., Timpu, F., Vogler-Neuling, V. V., Savo, R., & Grange, R. (2020). Barium Titanate Nanostructures and Thin Films for Photonics. Adv. Optical Mater, 8(2001249), 1-23. doi:DOI: 10.1002/adom.202001249.

Bhat, D. Krishna., Bantawal, Harsha., & Shenoy, U. Sandhya. (2020). Rhodium doping augments photocatalytic activity of barium titanate: effect of electronic structure engineering. Nanoscale Advances, 2(1), 5688–5698. DOI: 10.1039/d0na00702a.

M, l. F., T, Z., E, N. C., & J, M. (2023). Structural ,Infra-red and Morpphlogical effect of Sm+3 Dopeed Barium Titanate Nanoparticles. Nigerian Journal Physics, 32(1), 1-5.

Mahata, M. K., Koppe, t., Kumar, K., Hofsäss, H., & Vetter, U. (2020). Upconversion photoluminescence of Ho3+-Yb3+ doped barium titanate nanocrystallites: optical

tools for structural phase detection and temperature probing. Scientific RepoRtS, 10(8775), 1-12. doi:https://doi.org/10.1038/ s41598-020-65149-z.

ALEKSANDOVA, Mihaela., Lyuben, LAKOV., JIVOV, Bojidar & BLASKOV, Vladimir. (2021). Synthesis of La Doped Barium Titanate Ceramics with Application in Electronics. International Journal "NDT Days", IV(5). https://doi.org/10.1007/s00339-024-07381-2.

Marz ouk, S. Y., Azooz, M. A., Elsaghier, H. M., Zidan, N. A., & Abbas, W. (2022). Structural and optical properties of barium titanium borate glasses doped with ytterbium. J Mater Sci: Mater Electron, 33(01), 18054–18071. doi:https://doi.org/10.1007/s10854-022-08665-0.

Menasra, H., Adjal, F., Benbrika, C., Smaili, L., Bounab, K., Necira, Z., & Elfetni, A. (2024). Synthesis and Photocatalytic Activity of Zinc and Tungsten Co-Doped Barium Titanate Perovskite for Methylene Blue Degradation under Solar Irradiation. J.Chem.Soc.Pak, 46(03), 253-261. https://doi.org/10.1016/j.rinp.2020.103257.

More, S. P., Khedkar, M. V., Jadhav, S. A., Somvanshi, S. B., Humbe, A. V., & Jadhav, K. M. (2020). Wet chemical synthesis and investigations of structural and dielectric properties of BaTiO3 nanoparticles. Journal of Physics: Conference, 1644(012007), 1-9. doi:doi:10.1088/1742-6596/ 1644 /1/012007.

Nahar, A., Bhuiyan, M. A., Rahman, M. J., & Choudhury, S. (2021). Enhanced Dielectric properties of Bismuth Doped Barium Titanate Ceramics with their Structural and Compositional Studies. Biointerface Research in Applied Chemistry, 11(3), 9862-9870. https://doi.org/10.1016/j.heliyon.2022.e10529.

Nandi, M. (2020, August 30). Synthesis and Characterization of Carbon Coated Barium Titanate Core-Shell Nanoparticles. Missouri, Missouri State University, United States of American. https://doi.org/ 10.1016/ j.matchemphys.2020.124058.

Nguyen, T. (2020, July 15). Magneto-Electric Nanoparticles Cobalt Ferrite (CoFe2O4) – Barium Titnate (BaTiO3)for Non-invasive Neural Modulations. Bloomington, Indiana University, United States of America. https://doi.org/10.1016/j.matpr.2020.07.646.

Palusamy, R., Ganesan, T., Shajahan, A., Chandrasekaran, T., Sangilimuthu, A. y., & Umaralikhan, L. (2023, May-Aug). Structural, Optical, Antibacterial and Anticancer Properties Silver Barium Modifid Titanium Dioxide Nanoparticles Prepared via a Green Process Using Withania somnifera Hairy Roots. Asian Journal of Biological and Life Sciences, 12(2), 294-300. DOI: 10.1142/S2010135X21500028.

Phong, L. T., Dang, N. T., Dang, N. V., Nguyen, V.-Q., Manh, D. H., Nam, P. H., Phong, P. T. (2022). the Royal Society of Chemistry, 12(01), 6119–16130. doi:DOI: 10.1039/d2ra01411d.

Ping, S. Y., Nuang, S. L., Hans G. L, C., & Tzyy Haur, C. (2021). Incorporation of barium titanate nanoparticles in piezoelectric PVDF membrane. Journal of Membrane Science, 1-39. doi:https://doi.org/ 10.1016/ j. memsci. 2021.119861.

Razzak, A. A., Barbooti, M. M., & Mohammed, A. A. (2022). Preparation and Characterization of Barium Titanate Nano Particles Using Solution Combustion. American Academic Scientific Research Journal for Engineering, Technology, and Sciences, 88(1), 302-311. Retrieved from http://asrjetsjournal.org. https:// doi.org/ 10.1016/ j. inoche.2024.113675.

S. Alex Pandian, M. Sivakumar. (2023). Barium titanate perovskite nanoparticles integrated reduced graphene oxide nanocomposite photoanode for high performance dye-sensitized solar cell. Results in Chemistry, 1(6), 101-109. doi:doi.org./ 10.1016/ j.rechem .2013 . 101091.

Saxena, N., Sharma, V., Sharma, R., Sharma, K. K., & Jain, K. K. (2021). The Effect of Thermal Annealing on Structural, Morphological and Optical Features of BaTiO3 Thin Film Prepared by e-Beam PVD Technique. Iranian Journal of Materials Science and Engineering, 18(01), 1-12. doi:DOI: 10.22068/ijmse.1879.

Sumanasinghe, V. A. (2023, March 30). Poling of Barium Titanate Nanoparticles-Incorporated Piezoelectric Paper Substrates. London, The Universiry OF Brtish Columbia, United Kingdom. https://dx.doi.org/10.4314/dujopas.v9i3a.13.

Tihtih, M., Ibrahim, J. F., Basyooni, M. A., Belaid, W., Gömze, L. A., & Kocserha, I. (2022, Aug 01). Structural, optical, and electronic properties of barium titanate: experiment characterisation and first-principles study. Materials Technology and Advanced Performance Materials, 01(01), 1-13. doi:DOI: 10.1080/10667857.2022.2107473.

Tihtih, M., M Ibrahim, F. J., Kurovics, E., & Abdelfattah, M. (2020). Study on the effect of Bi dopant on the structural and optical properties of BaTiO3 nanoceramics synthesized via sol-gel method. Journal of Physics: Conference, 1527(012043), 1-8. doi:doi:10.1088/1742-6596/1527/1/012043.

Tomar, R., Pandey, R., Singh, N. B., Gupta, M. K., & Gupta, P. (2020). Electrical properties of barium titanate in presence of Sn2+ dopant. SN Applied Sciences, 2(226), 1-7. doi:https:// doi.org/ 10.1007/ s42452-020-2017-8.

Ul Haq, E., Abdul Karim, M. R., Khan, K. I., Akram, W., Hassan, S. S., & Kashif, F. (2022). Study of structural and electrical properties of Zn-doped barium titanate ceramics synthesized by conventional solid-state method. Journal of Optoelectronics and Advanced Materals, 24(1 -2), 69-73. doi: 10.13168/cs.2024.0049.

Yoon, Y. n., Lee, D.-S., park, H. J., & Kim, J.-S. (2020). Barium titanate nanoparticles Sensitise treatment-Resistant Breast cancer cells to the Antitumor Action oftumour treating fields. Scientific RepoRtS, 10(2560), 1-9. doi: https://doi.org/10.1038/s41598-020-59445-x.

Zhang, S., Fei, T., Cheng, T., Yang, J.-Y., & Liu, L. (2023). Temperature- dependedent UV-Visible dilelctricfunctions of BaTiO3 across ferroelectric-paraelectric phase transition. Optics Express, 31(08), 12357-12366 . doi:https://doi.org/10.1364/OE.486729.

Alshoaibi, Adil., Kanoun, Mohammed. Benali., Ul Haq, Bakhtiar., & AlFaify, Salem. (2020). Ytterbium doping effects into the Ba and Ti sites of perovskite barium titanate: Electronic structures and optical properties. Results in Physics, 18(1), 1-8. https:// doi.org/ 10.1016/ j.rinp.2020.103257.

Zhou, J. (2022, December 30). Characterization of Barium Titanate and Strontium Titanate Nanoparticles Synthesized by Hydrothermal and Molten-Salt Methods. California, University of California San Diego, United States of American. https://doi.org/ 10.1016/ j.vacuum. 2019 .04.047.